

DESY 99-182  
December 1999

# Probe of the $Wtb$ coupling in $t\bar{t}$ pair production at Linear Colliders

E. Boos<sup>1,2</sup>, M. Dubinin<sup>1,2</sup>, M. Sachwitz<sup>2</sup>, H.J. Schreiber<sup>2</sup>

<sup>1</sup>*Institute of Nuclear Physics, Moscow State University  
119899, Moscow, Russia*

<sup>2</sup>*DESY-Zeuthen, D-15738 Zeuthen, Germany*

## Abstract

The  $Wtb$  vertex can be probed on future colliders in the processes of single top production (LHC,  $pp$  mode, NLC,  $\gamma e$  mode) and of top pair production (NLC,  $e^+e^-$  mode). We analyse observables sensitive to anomalous  $Wtb$  couplings in the top pair production process of  $e^+e^-$  collisions. In particular, forward-backward and spin-spin asymmetries of the top decay products and the asymmetry of the lepton energy spectrum are considered. Possible bounds on anomalous couplings obtained are competitive to those expected from the upgraded Tevatron and LHC. The validity of the infinitely small width approximation for the three-body top decay is also studied in detail.

# 1 Introduction

One of the primary tasks for the forthcoming hadronic and leptonic colliders is a detailed study of the top quark properties, in particular, the measurements of the top couplings to gauge fields. Special interest to such measurements is based on the huge difference of the top quark mass and all other fermion masses, providing enhanced expectations for a signal of new physics at the top mass scale [1].

Among the top couplings to other particles the  $Wtb$  coupling plays a crucial role because it is responsible for practically all top quark decays. Therefore the spacetime structure of the  $Wtb$  vertex defines the top total width and the characteristics of its decay products.

There are two general possibilities to probe and measure directly the  $Wtb$  vertex structure in collider experiments, either from top pair production processes or from reactions of single top production. The rate of single top production processes is directly proportional to the  $Wtb$  coupling, and thus it is potentially very sensitive to the  $Wtb$  structure. This was indeed demonstrated in high energy  $\gamma e$  collisions [2, 3] as well as for the upgraded Tevatron and the LHC [4]. However, the rate of single top production is usually less than the top pair production rate, in both the lepton and hadron colliders. On the other hand, the reaction  $e^+e^- \rightarrow t\bar{t} \rightarrow W^+bW^-\bar{b}$  includes the  $Wtb$  coupling only in the subsequent top decays, with the  $t(\bar{t})$  on-shell decay rate given, apart from small finite width corrections, by the top decay branching fraction to  $Wb$ , which is close to 100%. Consequently, the total rate depends only negligibly on the  $Wtb$  vertex structure [2] and more sensitive observables, like  $C$  and  $P$  asymmetries, top polarization and spin correlations, have to be analysed.

The paper starts with the analysis of the process  $e^+e^- \rightarrow t\bar{t} \rightarrow W^+bW^-\bar{b}$  in the infinitely small width approximation, including anomalous couplings in the  $Wtb$  vertex. The narrow-width approximation enables qualitative interpretations of precise calculations presented later in this study. In Sect. 4 we perform precise tree-level computations in the Standard Model (SM) and in the generalization with the effective  $Wtb$  vertex. Asymmetries, energy distributions and spin-spin correlations are studied, including the option of electron beam polarization. In Sect. 5 the bounds of the anomalous coupling parameter space, within those no distinction from the SM is possible, are presented and compared with the corresponding limits obtained from single top production processes at NLC in the  $\gamma e$  mode and LHC in the  $pp$  mode.

## 2 Effective $Wtb$ lagrangian and the anomalous couplings $f_{2L}$ , $f_{2R}$

In the effective lagrangian approach seven gauge invariant and  $CP$  parity conserving operators of dimension six [5, 6] contribute to the  $Wtb$  vertex with four independent formfactors. In our analysis we use the effective lagrangian in the unitary gauge as given in [2, 4, 7]

$$\mathcal{L} = \frac{g}{\sqrt{2}} \left[ W_\mu^- \bar{b} (\gamma_\mu f_{1L} P_- + \gamma_\mu f_{1R} P_+) t - \frac{1}{2M_W} W_{\mu\nu} \bar{b} \sigma^{\mu\nu} (f_{2R} P_- + f_{2L} P_+) t \right] + \text{h.c.} \quad (1)$$

where  $W_{\mu\nu} = D_\mu W_\nu - D_\nu W_\mu$ ,  $D_\mu = \partial_\mu - ieA_\mu$ ,  $P_\pm = 1/2(1 \pm \gamma_5)$  and  $\sigma^{\mu\nu} = i/2(\gamma_\mu\gamma_\nu - \gamma_\nu\gamma_\mu)$ .

In the SM, the coupling  $f_{1L}$  is equal to one and the other three couplings,  $f_{1R}$ ,  $f_{2L}$  and  $f_{2R}$ , are equal to zero. The possible (V+A) coupling  $f_{1R}$  is severely constraint to zero by the CLEO  $b \rightarrow s\gamma$  data [8] on a level [6, 9] which is stronger than expected even at high energy  $\gamma e$  colliders. So in the following, we set  $f_{1R} = 0$  and  $f_{1L} = 1$  due to the fact that the (V-A) coupling is as in the SM with the coupling  $V_{tb}$  very close to unity, as required by present data [10]. This leaves us to perform the analysis only for the two 'magnetic' anomalous couplings  $f_{2L}$  and  $f_{2R}$ .

The couplings  $f_{2L}$  and  $f_{2R}$  are related to the effective couplings  $C_{tW\Phi}$  and  $C_{bW\Phi}$  [6] in the general effective lagrangian by

$$f_{2L(R)} = \frac{C_{t(b)W\Phi}}{\Lambda^2} \frac{v\sqrt{2}m_W}{g} \quad (2)$$

where  $\Lambda$  is the scale of new physics. Future Tevatron data (Run 3) should limit  $|C_{tW\Phi}|/(\Lambda/TeV)^2$  to  $\sim 0.6$  [11], which in turn corresponds to upper limits for  $|f_{2L(R)}|$  of the order of 1.

In all our calculations which follow the Feynman rules in the momentum space corresponding to the effective lagrangian (1) were implemented in the program package CompHEP [12].

## 3 Parity violating observables in the top decay

It is straightforward to demonstrate by direct calculation that, as mentioned in the introduction, the total rate of the process  $e^+e^- \rightarrow t\mu^-\bar{\nu}_\mu\bar{b}$  is weakly dependent on the anomalous couplings  $f_{2L}$  and  $f_{2R}$ . For instance, if  $(f_{2L}, f_{2R}) =$

(-0.6, 0), the total cross section at  $\sqrt{s} = 500$  GeV equals 62.7 fb, while the SM value is 63.0 fb. The effect of non-zero  $f_{2L,R}$  couplings in the amplitude is largely compensated by the increase of the top quark width ( $\Gamma_{top}=1.60$  GeV in the standard case and 4.35 GeV at  $(f_{2L}, f_{2R})=(-0.6, 0)$ ). Hence, the observation of nonstandard interactions is only possible in variables which are sensitive to the effective lagrangian terms (1). It is however *a priori* not evident which variables provide sufficiently high sensitivity to anomalous  $Wtb$  operators, so that we are prompted to look, as a first example, for the forward-backward asymmetry of top decay products which is the ratio of integrated single differential distributions.

### 3.1 Forward-backward asymmetry in the infinitely small width approximation

In the usual approach to the reaction  $e^+e^- \rightarrow t\bar{t} \rightarrow 6$  fermions, the final state topology is calculated in the approximation of infinitely small top and  $W$  widths

$$\frac{1}{(q^2 - m^2)^2 + m^2 \Gamma^2} = \frac{1}{m \Gamma} \delta(q^2 - m^2) . \quad (3)$$

Representations of the general expression for distributions in the  $W^+W^-b\bar{b}$  final state in terms of the unpolarized  $t\bar{t}$  cross section  $\Sigma_{unpol}$ , factorized top-antitop branching ratios, polarization functions  $P, \bar{P}$  of the  $t, \bar{t}$  and the  $t\bar{t}$  spin-spin correlation function  $Q$  can be found in [13, 14], see also [15]. They can be obtained from the convolution of the  $t\bar{t}$  production amplitude with the amplitude density matrices of the  $t \rightarrow W^+b$  and  $\bar{t} \rightarrow W^-b$  decays. Following the notations of [13] one gets

$$\begin{aligned} & \frac{d^4\sigma(e^+e^- \rightarrow t\bar{t} \rightarrow W^+bW^-\bar{b})}{d\cos\Theta d\cos\theta d\varphi d\cos\theta^* d\varphi^*} \\ &= \frac{3\alpha^2\beta}{32\pi s} Br(t \rightarrow W^+b) Br(\bar{t} \rightarrow W^-\bar{b}) \Sigma(\Theta, \theta, \varphi, \theta^*, \varphi^*) , \end{aligned} \quad (4)$$

where  $\Theta$  is the top production angle,  $\beta = \sqrt{1 - 4m_t^2/s}$  and

$$\begin{aligned} \Sigma(\theta, \varphi, \theta^*, \varphi^*) &= \Sigma_{unpol} + k P \cos\theta + \bar{k} \bar{P} \cos\theta^* + \cos\theta \cos\theta^* k \bar{k} Q \\ &+ (\varphi, \varphi^* \text{ dependent terms}). \end{aligned} \quad (5)$$

The angles  $\theta, \varphi/\theta^*, \varphi^*$  define the  $W$  momentum direction in the rest frame of the top/antitop. The definitions of these angles can be found in the Appendix. In the following, integrations over the azimuthal angles  $\varphi, \varphi^*$  will be always carried out, with the result that  $\varphi, \varphi^*$  dependent terms are equal to zero. The variables  $k$  and  $\bar{k}$  are the polarization degree of the top and antitop decay amplitudes. The expressions for  $\Sigma_{unpol}, P, \bar{P}$  and  $Q$  in terms of the helicity

amplitudes  $\langle \sigma; h_t h_{\bar{t}} \rangle$  for  $t\bar{t}$  production have the form

$$\Sigma_{unpol} = \frac{1}{4} \int d\cos\Theta \sum_{\sigma=\pm} \left[ |\langle \sigma; ++ \rangle|^2 + |\langle \sigma; +- \rangle|^2 + |\langle \sigma; -+ \rangle|^2 + |\langle \sigma; -- \rangle|^2 \right] \quad (6)$$

$$P = \frac{1}{4} \int d\cos\Theta \sum_{\sigma=\pm} \left[ |\langle \sigma; ++ \rangle|^2 + |\langle \sigma; +- \rangle|^2 - |\langle \sigma; -+ \rangle|^2 - |\langle \sigma; -- \rangle|^2 \right] \quad (7)$$

$$\bar{P} = \frac{1}{4} \int d\cos\Theta \sum_{\sigma=\pm} \left[ |\langle \sigma; ++ \rangle|^2 - |\langle \sigma; +- \rangle|^2 + |\langle \sigma; -+ \rangle|^2 - |\langle \sigma; -- \rangle|^2 \right] \quad (8)$$

$$Q = \frac{1}{4} \int d\cos\Theta \sum_{\sigma=\pm} \left[ |\langle \sigma; ++ \rangle|^2 - |\langle \sigma; +- \rangle|^2 - |\langle \sigma; -+ \rangle|^2 + |\langle \sigma; -- \rangle|^2 \right] \quad (9)$$

where (see, for instance, [14])

$$\langle - \mp \pm \rangle = \mp(v_L \mp \beta a_L)(1 \pm \cos\Theta) \quad (10)$$

$$\langle - \mp \mp \rangle = \pm \frac{2m_t}{\sqrt{s}} v_L \sin\Theta \quad (11)$$

$$\langle + \mp \pm \rangle = \pm(v_R \mp \beta a_R)(1 \mp \cos\Theta) \quad (12)$$

$$\langle + \mp \mp \rangle = \pm \frac{2m_t}{\sqrt{s}} v_R \sin\Theta, \quad (13)$$

and  $v_{L,R}$  and  $a_{L,R}$  are the standard vector and axial couplings of the  $\gamma$  and  $Z$  to the electron and top quark currents. Numerical values of  $P$ ,  $\bar{P}$  and  $Q$ , in units of  $\Sigma_{unpol}$ , at  $\sqrt{s}=500$  GeV and integrated over  $\Theta$  are

$$\Sigma_{unpol} : P : \bar{P} : Q = 1 : -0.18 : 0.18 : -0.63 \quad (14)$$

Thus, the spin-spin correlation term  $Q$  in eq.(5) is expected to be significant; it is found to be about four times larger than the polarization function  $P$ . The ratio  $Q/P$  depends weakly on  $\sqrt{s}$  in the range from 360 to about 1000 GeV, so that for a  $\Sigma_{unpol}$  variation in this energy range by approximately a factor of two to three, our analysis is not critically dependent on  $\sqrt{s}$ . Throughout the paper we have chosen  $\sqrt{s}=500$  GeV.

The polarization degrees  $k$  and  $\bar{k}$  of the  $t$  and  $\bar{t}$  decay amplitudes, summed over the  $W$  helicity states, are defined by the structure of the  $Wtb$  vertex. If the spin quantization axis is collinear to the top momentum, the  $t \rightarrow W^+b$  amplitude polarization density matrix in the rest frame of the top has the form ([7], see details in the Appendix)

$$\frac{1}{2} \begin{pmatrix} 1 + k \cos\theta & k \sin\theta e^{i\varphi} \\ k \sin\theta e^{-i\varphi} & 1 - k \cos\theta \end{pmatrix} \quad (15)$$

The explicit expression for the polarization degree  $k$  for the  $t \rightarrow W^+b$  decay can be obtained in models with the general effective lagrangian (1) by means

of the eight helicity amplitudes of the top decay defined in the Appendix. In the case  $f_{1L}=1$ ,  $f_{1R}=0$  we get

$$k = \frac{\left(\frac{m_t}{m_W} + f_{2L}\right)^2 - 2\left(1 + \frac{m_t}{m_W} f_{2L}\right)^2 - \left(1 - 2\left(\frac{m_t}{m_W}\right)^2\right) f_{2R}^2}{\left(\frac{m_t}{m_W} + f_{2L}\right)^2 + 2\left(1 + \frac{m_t}{m_W} f_{2L}\right)^2 + \left(1 + 2\left(\frac{m_t}{m_W}\right)^2\right) f_{2R}^2} \quad (16)$$

The expressions (4), (5), (16) provide the basis for a qualitative understanding of the results from exact matrix element Monte Carlo calculations, when nonzero bottom quark mass and finite top quark and  $W$ -boson widths are accounted for.

It follows from (5) that natural integrated angular observables are the  $b$ -quark and the lepton forward-backward asymmetries, measured in the rest frame of the top. It is straightforward to show that these asymmetries have the form

$$A_{FB} = \frac{\sigma(\theta < 90^\circ) - \sigma(\theta > 90^\circ)}{\sigma(\theta < 90^\circ) + \sigma(\theta > 90^\circ)} = \frac{k}{2} \frac{P}{\Sigma_{unpol}} \quad (17)$$

For the  $b$ -quark, the polarization degree  $k$  in the SM equals 0.41 (see the Appendix) and the ratio  $P/\Sigma_{unpol}$  (the degree of longitudinal top quark polarization integrated over  $\Theta$ ) is equal to 0.18<sup>1</sup> at  $\sqrt{s} = 500$  GeV. Hence,  $A_{FB}^b$  in the infinitely small width approximation equals 3.6%, while for the lepton from  $W$  decay, with  $k=1$  in the SM,  $A_{FB}^l = -9.0\%$ .

### 3.2 Infinitely small $W$ width approximation in the top quark anomalous decay

The effective lagrangian terms of the  $Wtb$  vertex can significantly change the top quark two-body and three-body decay widths if the anomalous couplings  $f_{2L}$ ,  $f_{2R}$  are sufficiently large. Whether however finite  $W$  width corrections substantially obscure effects of anomalous couplings demands to investigate computations done within approximation (3) and to reveal its relation to exact Breit-Wigner propagator calculations. In order to quantify this question we performed an explicit symbolic calculation of the factorized branching ratios in formula (4). The result for the two-body top decay width can be obtained from the helicity amplitudes (30)-(37):

$$\Gamma_2(t \rightarrow W^+ b) = \frac{G_F m_t^3}{8\sqrt{2} \pi} (1 - r^2)^2 [1 + 2r^2 + 6 f_{2L} r + (f_{2L}^2 + f_{2R}^2)(2 + r^2)] \quad (18)$$

where  $r = m_W/m_t$ . The three-body top decay width, after integration of the symbolic expression over the Dalitz plot, is given by

$$\begin{aligned} \Gamma_3(t \rightarrow e^+ \nu_e b) = & \frac{G_F^2 m_t^3 m_W^2}{96\pi^3} \left[ F_1 \frac{m_W}{\Gamma_W} \left( \pi - \arctan \frac{m_W^2 \Gamma_W}{m_W(m_t^2 - m_W^2 - \Gamma_W^2)} \right) \right. \\ & \left. + F_2 \log \frac{m_W^2 (m_W^2 + \Gamma_W^2)}{(m_t^2 - m_W^2)^2 + m_W^2 \Gamma_W^2} + F_3 \right] \end{aligned} \quad (19)$$

---

<sup>1</sup>The  $P$  dependence on the top production angle can be found in [15, 16].

where

$$\begin{aligned}
F_1 &= 1 - 3r^4 + 2r^6 + 3r^2\gamma^2 - 6r^4\gamma^2 \\
&\quad - 6f_{2L}(2r^3 - r^5 - \gamma - 2r\gamma^2 + 3r^3\gamma^2) \\
&\quad + (f_{2L}^2 + f_{2R}^2)(2 - 3r^2 + r^6 + 3\gamma^2 - 6r^4\gamma^2 + r^2\gamma^4) \\
F_2 &= 3r^4 - 3r^6 + r^4\gamma^2 - 3f_{2L}(r - 4r^3 + 3r^5 - r^3\gamma^2) \\
&\quad + (f_{2L}^2 + f_{2R}^2)(-1 + 3r^2 - 2r^6 + 2r^4\gamma^2) \\
F_3 &= -3r f_{2L}(3 - 4r^2) + (f_{2L}^2 + f_{2R}^2)(-\frac{1}{3} + r^2 + 3r^4 - r^2\gamma^2)
\end{aligned}$$

and  $\gamma = \Gamma_W/m_t$ . If we set  $f_{2L} = f_{2R} = 0$  and use the approximation  $F_1 = 1 - 3r^4 + 2r^6$  and neglect  $\Gamma_W/m_t$  power terms, we obtain by comparing (18) and (19) the explicit narrow width factorization in the SM case:

$$\begin{aligned}
\Gamma_3(t \rightarrow e^+ \nu_e b) &= \frac{G_F^2 m_t^3 m_W^3}{96\pi^3} \frac{\pi}{\Gamma_W} (1 - 3r^4 + 2r^6) = \\
&= \frac{G_F m_t^3}{8\sqrt{2}\pi} (1 - r^2)^2 (1 + 2r^2) \frac{1}{\Gamma_W} \frac{G_F m_W^3}{6\sqrt{2}\pi} = \Gamma_2(t \rightarrow W^+ b) \text{Br}(W^+ \rightarrow e^+ \nu_e)
\end{aligned} \tag{20}$$

Since the  $W$  branching factorisation (20) is in general not valid, its violation by  $f_{2L,R} \cdot \Gamma_W/m_t$  and  $f_{2L,R} \cdot m_W/m_t$  power terms is only weak provided modulus of  $f_{2L}$  and  $f_{2R}$  are around or less than 1. More details about the precision of the factorization approximation can be obtained from Fig.1, where the ratio  $\Gamma_3/(\Gamma_2 \cdot \text{Br}(W^+ \rightarrow e^+ \nu_e))$  as a function of the anomalous couplings  $f_{2L}$  and  $f_{2R}$  is shown. Clearly, the accuracy of  $\Gamma_3$  within the infinitely small  $W$  width approximation is convincing in the range considered for  $f_{2L}$  and  $f_{2R}$ ; deviations are expected to be of the order 1% or less. Thus, calculations done within the approximation (3) imply small corrections which are less important than e.g. interferences between the signal diagrams (see below). In general, however, careful investigations are appropriate when anomalous top quark decay calculations are carried out within the infinitely small  $W$  width approximation.

## 4 Tree-level results for $e^+ e^- \rightarrow t\bar{t} \rightarrow tl\bar{\nu}_l\bar{b}$

If precise measurements of top decay products are envisaged, it is demanding to know the SM predictions with very high accuracy. The program package CompHEP [12] which performs analytic calculations of the matrix element squared, generates an optimized FORTRAN code and generates an event flow, overcomes the shortcomings due to infinitely small width and zero fermion mass approximations. Furthermore, it allows to include all diagrams of the irreducible background and their interferences. In the case of the signal process,  $e^+ e^- \rightarrow t\bar{t} \rightarrow tl\bar{\nu}_l\bar{b}$ , only two diagrams and their interference exist. If the

anomalous couplings  $f_{2L}$  and  $f_{2R}$  are allowed to contribute to the lagrangian, the corresponding Feynman rules implemented in CompHEP can be found in the Appendix of the second ref. in [2].

## 4.1 Forward-backward asymmetries

It follows from eqs.(4) and (5) that observables of experimental interest are the distributions in  $\theta$ ,  $\theta^*$  for the  $b$ -quark and lepton in the top rest frame, or in the  $e^+e^-$  center-of-mass system (c.m.s.) for a more general discussion. From these distributions the forward-backward asymmetry (17) can be easily calculated in the SM and in models extended by anomalous couplings.

In a first step we compare precise calculations with results obtained from the infinitely small width approximation (3), within the SM ( $f_{2L} = f_{2R} = 0$ ). Numerical values for the  $b$ -quark and lepton asymmetries,  $A_{FB}^b$  and  $A_{FB}^l$ , calculated by means of CompHEP, are shown in Table 1, in the top rest frame as well as in the  $e^+e^-$  c.m.s. If compared with the top rest frame asymmetries obtained within the narrow width approximation of sect.3.1, one notices a 15% difference for the  $b$ -quark, whereas for the lepton the difference is negligible. Thus, already this example demonstrates the importance of precise calculations which include interference terms, finite width and non-zero mass contributions.

The SM forward-backward  $b$ -quark asymmetries (Table 1) are significantly larger in the  $e^+e^-$  c.m.s. than in the top rest frame, while for the lepton such differences are less evident. This observation can be understood by recalling that the  $t$  ( $\bar{t}$ ) is produced mainly in the  $e^-$  ( $e^+$ ) direction with left (right) helicity and, in the top decay, the lepton ( $b$  quark) is emitted preferably in the direction of (in the opposite direction to) the top spin.

It is also worth to mention that irreducible background, which might remain after any  $t\bar{t}$  selection procedure, should be carefully accounted for. CompHEP calculation shows that if the electron being the lepton in the final state (with 18 contributing diagrams in total) forward electrons from  $t$ -channel photon exchange alter significantly  $A_{FB}^e$  compared to only signal diagrams calculations.

When we allow for anomalous  $Wtb$  couplings, the asymmetry  $A_{FB}^b$ , measured in the top rest frame, is shown in Fig. 2 in the narrow width approximation and for exact calculations. The qualitative behaviour of both asymmetries as a function of  $f_{2L}$  and  $f_{2R}$  is very similar; only close inspections reveal significant differences. Furthermore,  $A_{FB}^b$  depends stronger on  $f_{2L}$  than on  $f_{2R}$ , as can be better seen in Fig.3a, where also two standard exclusion contour plots are shown for  $100 \text{ fb}^{-1}$  and  $500 \text{ fb}^{-1}$  integrated luminosities. This greater sensitivity is directly connected to the stronger influence of the linear  $f_{2L}$  term in (16) than that of the quadratic  $f_{2R}$  term, which in turn is an inherent property of the helicity amplitudes of anomalous top quark decays,

	$f_{2R}$	$f_{2L}$	$A_{FB}$ , $e^+e^-$ c.m.s.	$A_{FB}$ , top frame
unpolarized $e^+e^- \rightarrow t\mu\bar{\nu}_\mu b$				
$b$	0.0	0.0	0.279	0.030
$\bar{b}$	0.0	-0.2	0.243	0.010
$\bar{b}$	0.0	-0.4	0.218	-0.004
$\bar{b}$	0.0	-0.6	0.197	-0.020
$\bar{b}$	0.0	-1.0	0.169	-0.039
$b$	-0.6	0.0	0.301	0.041
$\bar{b}$	-1.0	0.0	0.315	0.045
$\mu$	0.0	0.0	0.079	-0.091
$\mu$	0.0	-0.6	0.085	-0.084
polarized $e_L^-e^+ \rightarrow t\mu\bar{\nu}_\mu b$				
$b$	0.0	0.0	0.354	0.100
$\bar{b}$	0.0	-0.2	0.265	0.034
$\bar{b}$	0.0	-0.4	0.200	-0.011
$\bar{b}$	0.0	-0.6	0.152	-0.047
$\bar{b}$	0.0	-1.0	0.087	-0.095
$\mu$	0.0	0.0	0.145	-0.262
$\mu$	0.0	-0.6	0.104	-0.233

Table 1: Forward-backward asymmetries for the  $b$ -quark and lepton in the reaction  $e^+e^- \rightarrow t\bar{l}^-\bar{\nu}_l\bar{b}$  at  $\sqrt{s} = 500$  GeV, for the standard and anomalous effective  $Wtb$  vertices, calculated in the  $e^+e^-$  center of mass frame and in the top rest frame.

as outlined in the Appendix.

The impact of the anomalous couplings to the lepton forward-backward asymmetry  $A_{FB}^l$  is less important both in the  $e^+e^-$  c.m.s. and the top rest frame (see Fig.3b), and being only indirect due to the presence of the standard left current  $W$  boson decay. However, in contrast to the two-fold ambiguity of the  $b$ -quark asymmetry (Fig. 3a),  $A_{FB}^l$  is unique in the sense that for a given  $f_{2R}$  value only one  $f_{2L}$  range (shaded) exists, in which no distinction from the SM (within  $2\sigma$ ) is possible.

Table 1 contains some numerical examples of  $A_{FB}^{b/l}$  for several  $f_{2L}$  and  $f_{2R}$  values at  $\sqrt{s} = 500$  GeV, measured in both reference frames discussed so far. Clearly, the largest forward-backward asymmetry is obtained for the  $b$  quark if measured in the  $e^+e^-$  c.m.s. One should however remember that  $e^+e^-$  c.m.s. asymmetries are a superposition of production and decay asymmetries, while asymmetries reconstructed in the top rest frame can be considered as a 'pure' effect.

Left electron beam polarization not only increases the  $t\bar{t}$  production rate by a factor of about three ( $\sigma_{tot} = 176$  fb for 100% left polarized electrons at  $\sqrt{s} = 500$  GeV) but also enhances  $A_{FB}^{b/l}$  by a factor of 2-3 in the top rest frame. At the same time, the  $f_{2L}$  sensitivity of  $A_{FB}^b$  increases most significantly if measured in the  $e^+e^-$  c.m.s. (see the examples in Table 1).

Besides the study of the  $\theta$  and  $\theta^*$  decay angular distributions, more sophisticated angular observables were proposed to study parity violating effects: (1) the angle between the lepton momentum in the  $W$  rest frame and the momentum of the top in the  $e^+e^-$  c.m.s. [17] and (2) the angle between the top production plane and the production plane of the  $b$ -quark (or the lepton) in the  $e^+e^-$  c.m.s.:

$$\cos \theta_{tb} = \frac{(\mathbf{kt} \cdot \mathbf{kb})}{\|\mathbf{kt}\| \|\mathbf{kb}\|} , \quad (21)$$

where  $\mathbf{k}$  is a unit length vector in the  $e^-$  direction. A similar variable was proposed in [18] to measure the transverse quark polarization.

In both angular distributions very large asymmetries (up to 95%) exist. However, their sensitivity to the anomalous  $Wtb$  couplings  $f_{2L}$  and  $f_{2R}$  is very small and is, in good approximation, independent on the electron polarization.

## 4.2 Energy spectrum asymmetry

Besides angular distributions, energy spectra of the top decay products may also possess high sensitivity to anomalous couplings. In this section we study the asymmetry of the lepton energy spectrum defined in the top rest frame using the dimensionless variable  $x_\mu = 2E_\mu/m_{top}$ :

$$A_E^\mu = \frac{\sigma(x_\mu < 0.5) - \sigma(x_\mu > 0.5)}{\sigma(x_\mu < 0.5) + \sigma(x_\mu > 0.5)} \quad (22)$$

Fig.3c shows the results for  $A_E^\mu$  from the process  $e^+e^- \rightarrow t\mu\bar{\nu}_\mu\bar{b}$  as a function of  $f_{2L}$  and  $f_{2R}$ . As can be seen,  $A_E^\mu$  is significantly more sensitive to  $f_{2L}$  than its forward-backward asymmetry  $A_{FB}^\mu$ , and this result is independent whether  $A_E^\mu$  is measured in the top rest frame or in the  $e^+e^-$  c.m.s. Alike to  $A_{FB}^b$ , the sensitivity to  $f_{2R}$  is somewhat less pronounced than to  $f_{2L}$  and the ambiguity exists also.

The  $b$ -quark energy spectrum in the top rest frame has a resonance peak at  $x_b = 1 - (m_W/m_t)^2$ , resulting to an energy asymmetry insensitive to anomalous couplings.

If the neutrino is used as the analyser (by means of the missing energy technique), its energy asymmetry is slightly less sensitive to  $f_{2L}$  and  $f_{2R}$  than the lepton energy asymmetry. Whether the neutrino is at all usable for precise measurements, requires however detailed experimental studies including full event simulation and reconstruction.

As clearly visible from Figs.3a-c, only the combination of forward-backward and energy asymmetry measurements results to an allowed region (Fig.4, the sum of the grey and dark areas) much smaller than that for each measurement alone and ensures a significant improvement of the sensitivity on anomalous couplings, with limits for  $f_{2L}$  and  $f_{2R}$  sensible luminosity dependent.

### 4.3 Spin-spin asymmetries

The spin correlations and the spin-spin asymmetries, which are related to each other, are in general double differential distributions where one of the variables is integrated over a certain kinematical region. As already mentioned in sect. 3, the spin correlation term  $k\bar{k}Q$  in (5) is comparable to the polarization term  $kP$  and therefore spin-spin correlations, although suppressed by the additional power of  $k$ , are expected to be not small. For instance, the forward-backward asymmetry of the  $b$ -quark measured in the top rest frame, under the condition that the  $\bar{b}$ -quark is observed only in the forward hemisphere in the  $\bar{t}$  rest frame, can be derived from (5) as

$$A_s^b = \frac{k}{2} \frac{P}{\Sigma_{unpol}} \left(1 + \bar{k} \frac{Q}{2P}\right) \quad . \quad (23)$$

For simplicity, the term  $\bar{k}\bar{P}/\Sigma \ll 1$  is omitted here. At e.g.  $\sqrt{s} = 500$  GeV, we find  $A_s^b = 0.062$  within the SM, which is two times larger than  $A_{FB}^b = 0.036$ , when no restriction is imposed on the  $\bar{t}$  side.

If anomalous couplings are allowed to contribute, the dependence of the spin-spin asymmetry,  $A_s^b$ , on  $f_{2L}, f_{2R}$  is shown in Fig.5, within the narrow width approximation. Clearly, improved constraints on  $f_{2L}, f_{2R}$  can be obtained from  $A_s^b$  compared to the unrestricted forward-backward asymmetries as discussed in sect. 4.1. However, since  $A_s^b$  is calculated in the infinitely small width approximation<sup>2</sup>, the reliability of the results needs more careful investigation.

We expect some further enhancement of parity-violating effects by using polarized beams. If e.g. 100% left polarized electrons collide with unpolarized positrons, forward  $t$  (backward  $\bar{t}$ ) quarks (w.r.t. the  $e^-$  direction) are mainly produced in the helicity configuration L (R), while backscattered  $t$  (forward  $\bar{t}$ ) are produced in the helicity configuration R (L) (their production angular behaviour can be found in [19]). As a consequence, the  $t$  and  $\bar{t}$  decay products in the reaction

$$e^+e^- \rightarrow t\bar{t} \rightarrow (e^-\nu_e\bar{b})(u\bar{d}b)$$

are expected to be strongly correlated, in so far as the  $e^-$  and the  $\bar{d}$  are produced mainly in the top spin direction, while the u- and b-quarks prefer

---

<sup>2</sup>For reasons of unsufficient computer memory, CompHEP 2 → 6 calculations are only possible for the SM  $Wtb$  vertex, with the result  $A_s^b = 0.049$  at  $\sqrt{s} = 500$  GeV.

production in the opposite direction [20]. Using CompHEP to calculate the exact  $2 \rightarrow 6$  SM amplitudes, we obtain the electron decay angular distribution in the top rest frame under the condition that the  $\bar{d}$  decay angle in the antitop rest frame is less than  $90^\circ$ , for the top produced either forward (Fig. 6a) or backward (Fig. 6b) in the  $e^+e^-$  c.m.s. The spin-spin asymmetries in these two cases are -0.258 and -0.096, respectively, demonstrating strong sensitivity to parity-violating effects when beam polarization is available. QCD corrections to the spin correlations in  $t\bar{t}$  production are expected to be in general small [21], but their inclusion is recommended in searches for nonstandard interactions.

## 5 Conclusions

The total rate of the reaction  $e^+e^- \rightarrow t\bar{t} \rightarrow 6$  fermions at NLC energies is negligibly affected by the anomalous lagrangian terms (1). Hence, it is straightforward to use single and double differential distributions of the top/antitop decay products to eventually observe effects due to anomalous  $Wtb$  operators, and as larger their sensitivity as stronger limits on anomalous couplings can be imposed.

In this paper we investigate forward-backward asymmetries for the b-quark and the lepton in the top rest frame or in the  $e^+e^-$  c.m.s., the energy asymmetry of the lepton in the top rest frame and the spin-spin asymmetry in the  $t/\bar{t}$  decay. Precise tree-level Monte Carlo calculations for the signal diagrams and their interference were performed and compared in the case of forward-backward asymmetries with the symbolic expressions obtained in the infinitely small width and zero fermion mass approximation. We realized that in general careful investigations are appropriate when such approximations are intended to be used in analyses of multiparticle final state topologies.

Concerning the sensitivity of the observables considered in this study we found that (a)  $A_{FB}^b$ ,  $A_{FB}^l$  and  $A_E^l$  have stronger sensitivity to  $f_{2L}$  than to  $f_{2R}$ , as seen in Fig.3 <sup>3</sup>; (b) the sensitivity of the forward-backward b-quark asymmetry (Fig.3a) is larger than the sensitivity of the lepton forward-backward asymmetry (Fig.3b), which is somewhat degraded due to the subsequent  $W$  decay; (c) it is important to note that  $A_{FB}^l$  resolves the ambiguity observed in  $A_{FB}^b$  and  $A_E^l$ ; (d) the lepton energy asymmetry has the largest sensitivity on  $f_{2L}$  and  $f_{2R}$  (Fig.3c). In summary, it turns out that particle orientations seem to be less sensitive to anomalous  $Wtb$  operators than particle energies.

As indicated by the  $2\sigma$  exclusion contour plots in Figs. 3a-c, no satisfactory restriction on  $f_{2L}$  and  $f_{2R}$  has been obtained for each variable alone. But their combined annulus (Fig. 4) allows significant improvements of the sensi-

---

<sup>3</sup> For  $f_{1R} = 0$ , the helicity amplitudes (30)-(37) have linear and quadratic terms in  $f_{2L}$  and only quadratic terms in  $f_{2R}$ .

tivity on anomalous couplings. If in addition the spin-spin asymmetry of Fig. 5, although calculated within the narrow width approximation, is included, further restrictions on anomalous  $Wtb$  operators are possible for  $100 \text{ fb}^{-1}$  (dark area in Fig.4), while for  $500 \text{ fb}^{-1}$  no improvements are observed. Thus, for the high luminosity option of the TESLA linear collider [23] the bounds on the anomalous couplings  $f_{2L}$  and  $f_{2R}$ , within those no distinction from the SM is possible, are  $[-0.025, 0]$  for  $f_{2L}$  and  $\pm 0.20$  for  $f_{2R}$ . These rather promising results demonstrate the reliability of the top pair production process in  $e^+e^-$  collisions to probe the  $Wtb$  vertex.

It is interesting to compare these limits with the expectations from single top production processes at LHC [4]. The LHC limitations, being 2-3 times better than the possible restrictions from the upgraded Tevatron, are comparable to the  $e^+e^-$  LC estimates provided the LHC systematic uncertainties are controlled at a level better than about 10%. The advantage of the LHC to measure the single top production rates in the  $Wb\bar{b}/Wb\bar{b} + \text{jet}$  channels [4] is however somewhat degraded by relatively large uncertainties in the absolute normalization of the cross sections and the presence of reducible background not easy to control. In the clean environment of  $e^+e^-$  collisions, the selection of  $t\bar{t}$  events is thought to be very reliable and further improvements in probing the  $Wtb$  vertex can be expected if additional sensitive observables are included in the analysis and electron beam polarization is used. Whether however the superior sensitivity to the anomalous couplings  $f_{2L}$  and  $f_{2R}$  of a linear collider in the  $\gamma e$  mode at high energies ( $\sqrt{s_{e\gamma}} \geq 1 \text{ TeV}$ ) [2] could be achieved or even superseded, remains open for future studies.

### Acknowledgments

E.B. and M.D. are grateful to DESY-Zeuthen for hospitality. M.D. thanks very much H.S.Song for useful discussions. The work of E.B. and M.D. was partially supported by the RFBR-DFG grant 99-02-04011, the CERN-INTAS grant and the KCFE grant (SPb).

## Appendix

The helicity amplitudes for the decay  $t \rightarrow W^+b$  in models with the general interaction lagrangian (1) can be found in [7]. Our calculation follows the formalism of [22], where the chiral representation for the gamma matrices is used. The four component spinors can be split into two component helicity eigenstates  $\chi_\lambda(p)$

$$\begin{aligned} u(p, \lambda)_\pm &= \omega_{\pm\lambda}(p)\chi_\lambda(p) \\ v(p, \lambda)_\pm &= \pm\lambda\omega_{\mp\lambda}(p)\chi_{-\lambda}(p), \end{aligned} \tag{24}$$

where

$$\omega_{\pm}(p) = \sqrt{E \pm p}.$$

In the rest frame of the top, the helicity eigenstates of the  $b$ -quark can be written in the form

$$\chi_{+}(p_b) = \begin{pmatrix} \sin \frac{\theta}{2} \\ -\cos \frac{\theta}{2} e^{i\varphi} \end{pmatrix}, \quad \chi_{-}(p_b) = \begin{pmatrix} \cos \frac{\theta}{2} e^{-i\varphi} \\ \sin \frac{\theta}{2} \end{pmatrix} \quad (25)$$

with the following component representation of  $W$  and  $b$  momenta in the spherical coordinate system

$$p_W = \{E_W, |\mathbf{p}_W| \sin \theta \cos \varphi, |\mathbf{p}_W| \sin \theta \sin \varphi, |\mathbf{p}_W| \cos \theta\} \quad (26)$$

$$p_b = |\mathbf{p}_b| \{1, -\sin \theta \cos \varphi, -\sin \theta \sin \varphi, -\cos \theta\} \quad (27)$$

The polarization vectors of the  $W$  boson can be taken in the form

$$\begin{aligned} \epsilon_{+} &= \frac{1}{\sqrt{2}} \{0, -\cos \theta \cos \varphi + i \sin \varphi, -\cos \theta \sin \varphi - i \sin \varphi, \sin \theta\} \quad (28) \\ \epsilon_{-} &= \frac{1}{\sqrt{2}} \{0, \cos \theta \cos \varphi + i \sin \varphi, \cos \theta \sin \varphi - i \cos \varphi, -\sin \theta\} \\ \epsilon_0 &= \frac{E_W}{m_W} \left\{ \frac{|\mathbf{p}_W|}{E_W}, \sin \theta \cos \varphi, \sin \theta \sin \varphi, \cos \theta \right\} \end{aligned}$$

In the symbolic calculations we always neglect the  $b$ -quark mass. The eight helicity amplitudes  $\sqrt{2E_b m_t} \langle h_t, h_W, h_b \rangle$  corresponding to the matrix element of the top decay

$$\frac{g}{\sqrt{2}} \bar{u}(p_b) \Gamma_\mu u(p_t) \varepsilon_\mu^*(p_W)$$

with

$$\begin{aligned} \Gamma_\mu &= f_{1L} \gamma_\mu (1 - \gamma_5) + f_{1R} \gamma_\mu (1 + \gamma_5) \quad (29) \\ &+ \frac{f_{2L}}{2m_W} (\hat{p}_W \gamma_\mu - \gamma_\mu \hat{p}_W) (1 + \gamma_5) + \frac{f_{2R}}{2m_W} (\hat{p}_W \gamma_\mu - \gamma_\mu \hat{p}_W) (1 - \gamma_5) \end{aligned}$$

can be calculated in the rest frame of the top using (24)-(28):

$$\langle -, 0, - \rangle = \left( \frac{m_t}{m_W} f_{1L} + f_{2L} \right) \sin \frac{\theta}{2} \quad (30)$$

$$\langle -, -, - \rangle = \sqrt{2} \left( f_{1L} + \frac{m_t}{m_W} f_{2L} \right) \cos \frac{\theta}{2} \quad (31)$$

$$\langle +, 0, - \rangle = \left( \frac{m_t}{m_W} f_{1L} + f_{2L} \right) \cos \frac{\theta}{2} e^{i\varphi} \quad (32)$$

$$\langle +, -, - \rangle = -\sqrt{2} \left( f_{1L} + \frac{m_t}{m_W} f_{2L} \right) \sin \frac{\theta}{2} e^{i\varphi} \quad (33)$$

$$\langle +, 0, + \rangle = -\left(\frac{m_t}{m_W} f_{1R} + f_{2R}\right) \sin\frac{\theta}{2} \quad (34)$$

$$\langle +, +, + \rangle = \sqrt{2}\left(f_{1R} + \frac{m_t}{m_W} f_{2R}\right) \cos\frac{\theta}{2} \quad (35)$$

$$\langle -, 0, + \rangle = \left(\frac{m_t}{m_W} f_{1R} + f_{2R}\right) \cos\frac{\theta}{2} e^{-i\varphi} \quad (36)$$

$$\langle -, +, + \rangle = \sqrt{2}\left(f_{1R} + \frac{m_t}{m_W} f_{2R}\right) \sin\frac{\theta}{2} e^{-i\varphi} \quad (37)$$

The sum of the eight helicity amplitudes squared gives the total decay width of the top (18) for the general interaction lagrangian (1). If  $f_{1R}=0$ , the width  $\Gamma(t \rightarrow W^+ b)$  contains a linear term in  $f_{2L}$  and quadratic terms in both  $f_{2R}$  and  $f_{2L}$ . The eight helicity amplitudes of the antitop decay,  $\bar{t} \rightarrow W^- \bar{b}$ , can be obtained from (30)-(37) by the replacements  $f_{1L} \leftrightarrow f_{1R}$  and  $f_{2L} \leftrightarrow f_{2R}$  (only real  $f$  are considered). In the Standard Model (SM) with  $f_{1L}=1$ ,  $f_{1R} = f_{2L} = f_{2R}=0$  only four nonvanishing helicity amplitudes remain [14].

If  $(\theta, \varphi)$  are the polar and azimuthal angles of the  $b$ -quark with respect to the top momentum, the helicity amplitudes of the top with spin up and spin down,  $a_1$  and  $a_2$ , allow to define the  $t \rightarrow W^+ b$  amplitude polarization density matrix [7]. This matrix is different from the polarization density matrix defined by the individual top spin function. The squared sum of (32)-(35) gives the probability of spin up top decay, while the probability of spin down top decay is given by the squared sum of (30)-(31) and (36)-(37). The polarization density matrix can be defined for the  $(a_1, a_2)$  spin function

$$\rho = \begin{pmatrix} |a_1|^2 & a_1 a_2^* \\ a_1^* a_2 & |a_2|^2 \end{pmatrix}, \quad (38)$$

where the normalised SM components derived from (30)-(33) have the form

$$\begin{aligned} a_1^2 &= \frac{M_W^2}{m_t^2 + 2m_W^2} \left( \frac{m_t^2}{m_w^2} \cos^2 \frac{\theta}{2} + 2 \sin^2 \frac{\theta}{2} \right) \\ a_2^2 &= \frac{M_W^2}{m_t^2 + 2m_W^2} \left( \frac{m_t^2}{m_w^2} \sin^2 \frac{\theta}{2} + 2 \cos^2 \frac{\theta}{2} \right) \\ a_1 a_2^* = a_1^* a_2 &= \frac{m_t^2}{m_W^2} \sin^2 \frac{\theta}{2} + 2 \cos^2 \frac{\theta}{2} \end{aligned}.$$

The amplitude polarization density matrix (38) can also be represented in the standard form

$$\begin{aligned} \rho &= \frac{1}{2} \begin{pmatrix} 1 + k \cos \theta & k \sin \theta e^{i\varphi} \\ k \sin \theta e^{-i\varphi} & 1 - k \cos \theta \end{pmatrix} = \frac{I}{2} + \mathbf{P} \hat{\mathbf{S}} \\ &= \frac{1}{2} [I + k (\sin \theta \cos \varphi \sigma_1 + \sin \theta \sin \varphi \sigma_2 + \cos \theta \sigma_3)], \end{aligned} \quad (39)$$

where  $\hat{\mathbf{S}} = \{\sigma_1, \sigma_2, \sigma_3\}$  is the spin operator. The polarization vector  $\mathbf{P}$  is collinear to the  $b$ -quark momentum and the absolute value of the polarization vector, also called the polarization degree, is defined by the matrix element of the  $t \rightarrow W^+b$  decay. In the SM

$$k = \frac{m_t^2 - 2m_W^2}{m_t^2 + 2m_W^2} = 0.41 \quad .$$

In the case of a general interaction lagrangian the polarization degree depends on  $f_{2L,R}$  (see (16) in sect.3.1).

## References

- [1] R.D. Peccei, X. Zhang, Nucl.Phys. **B337**, 269 (1990)  
R.D. Peccei, S. Peris, X. Zhang, Nucl.Phys. **B349**, 305 (1991)
- [2] E. Boos, A. Pukhov, M. Sachwitz, H.J. Schreiber, Z.Phys. **C75**, 237 (1997); Phys.Lett. **B404**, 119 (1997).
- [3] J.-J. Cao, J.-X. Wang, J.-M. Yang, B.-L. Young, X. Zhang, Phys.Rev. D58 (1998) 094004.
- [4] E.Boos, L.Dudko, T.Ohl, report INP-MSU-99-4-562, 1999  
hep-ph/9903215, to appear in Eur. Phys. J.
- [5] W. Buchmüller, D. Wyler, Nucl. Phys. **B268**, 621 (1986);  
K. Hagiwara, S. Ishihara, R. Szalapski, D. Zeppenfeld, Phys. Rev. **D48**, 2182 (1993);  
K. Hagiwara, R. Szalapski, D. Zeppenfeld, Phys. Lett. **B318**, 155 (1993);  
B. Grzadkowski, J. Wudka, Phys. Lett. **B364**, 49 (1995);  
G.J. Gounaris, F.M. Renard, N.D. Vlachos, Nucl. Phys. **B459**, 51 (1996).
- [6] K. Whisnant, J.M. Yang, B.-L. Young, X. Zhang, Phys. Rev. **D56**, 467 (1997).
- [7] G.L. Kane, G.A. Ladinsky, C.-P. Yuan, Phys.Rev. **D45** (1992) 124.
- [8] M. Alam et al., CLEO Collaboration, Phys. Rev. Lett. **74**, 2885 (1995).
- [9] L. Larios, M.A. Perez, C.-P. Yuan, Phys.Lett. **B457** (1999) 334.
- [10] C. Caso et al., Particle Data Group, Eur.Phys.J. **C3** (1998) 1.
- [11] K. Hikasa, K. Whisnant, J. Yang, B. Young, Phys.Rev. **D58** (1998) 114003

- [12] E. Boos, M. Dubinin, V. Ilyin, A. Pukhov, V. Savrin, preprint INP MSU 94-36/358, 1994, hep-ph/9503280;  
 P.Baikov et.al, in: *Proc.of X Workshop on High Energy Physics and Quantum Field Theory*, ed. by B.Levtchenko, V.Savrin, Moscow, 1996, p.101;  
 A. Pukhov et.al., hep-ph/9908288;  
 see also <http://theory.npi.msu.su/~comphew>.
- [13] S.Y. Choi, A. Djouadi, H. Dreiner, J. Kalinowski, P.M. Zerwas, Eur. Phys. J. **C7** (1999) 123.
- [14] M.S. Baek, S.Y. Choi, C.S. Kim, Phys.Rev. **D56** (1997) 6835.
- [15] J.H. Kühn, A. Reiter, P.M. Zerwas, Nucl.Phys. **B272** (1986) 560.
- [16] T. Arens, L.M. Sehgal, Nucl.Phys. **B393** (1993) 46;  
 R.H. Dalitz, G.R. Goldstein, Phys.Rev **D45** (1992) 1531.
- [17] G.A. Ladinsky, C.-P. Yuan, Phys.Rev. **D49** (1994) 4415.
- [18] G.L. Kane, J. Pumplin, W. Repko, Phys.Rev.Lett. **41** (1978) 1689.
- [19] G. Mahlon, S. Parke, Phys.Rev. **D53** (1996) 4886;  
 S. Parke, Y. Shadmi, Phys.Lett. **B387** (1996) 199.
- [20] M. Jezabek, J.H. Kühn, Phys.Lett. **B329** (1994) 317.
- [21] A. Brandenburg, M. Flesch, P. Uwer, Phys.Rev. **D59** (1999) 014001.
- [22] K. Hagiwara, D. Zeppenfeld, Nucl.Phys. **B274** (1986) 1.
- [23] R.Brinkmann, preprint TESLA 99-15, to appear in: *Proc. of the Workshop on Physics and Experiments with Linear Colliders*, Sitges, Barcelona, 1999.

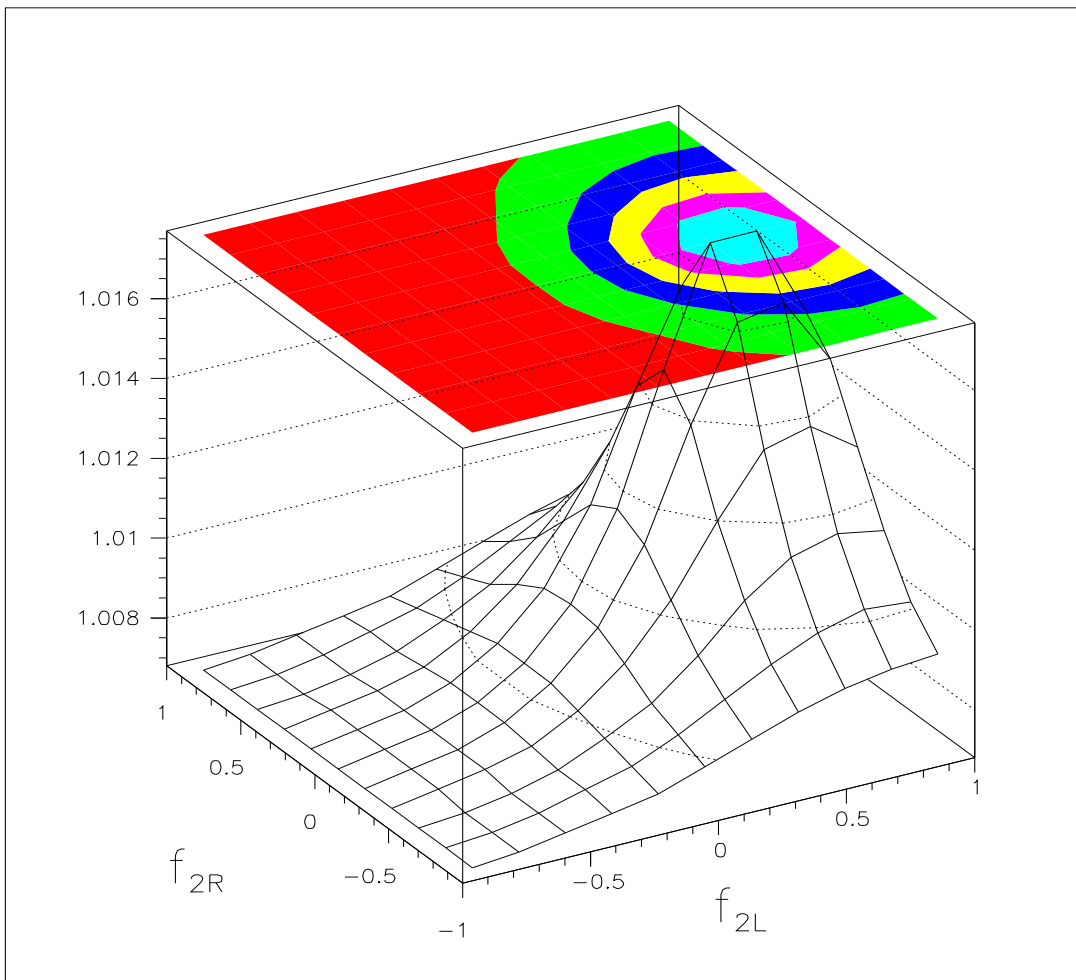


Figure 1: The ratio  $\Gamma_3(t \rightarrow e^+ \nu_e b) / (\Gamma_2(t \rightarrow W^+ b) Br(W^+ \rightarrow e^+ \nu_e))$  versus  $f_{2L}$  and  $f_{2R}$ , with equidistant isocontours in the  $f_{2L}, f_{2R}$  projection.

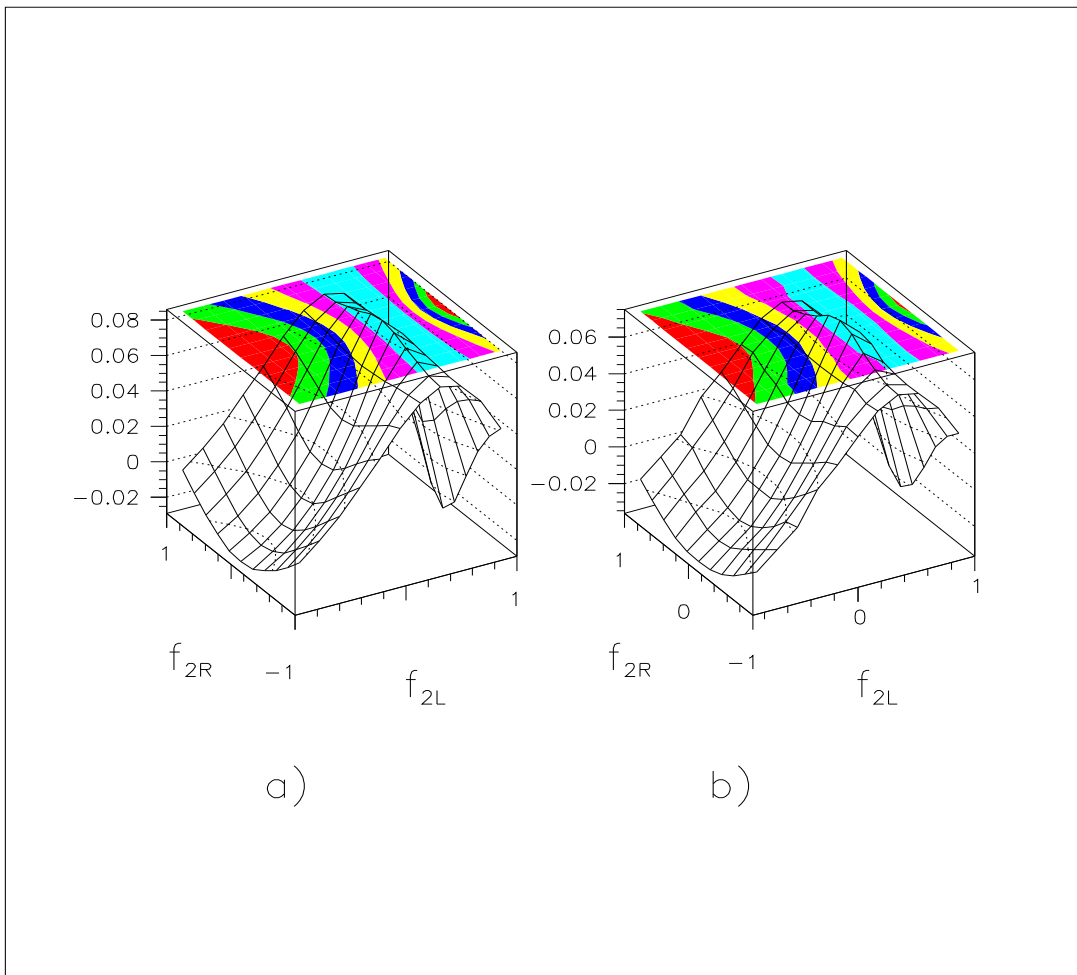


Figure 2: Forward-backward  $b$ -quark asymmetry in the top rest frame a) calculated within the infinitely small width approximation and b) precisely calculated using CompHEP, for the reaction  $e^+e^- \rightarrow t\bar{t} \rightarrow tl^-\bar{\nu}_l\bar{b}$  as a function of  $f_{2L}$  and  $f_{2R}$ .  $A_{FB}^b$ -equidistant isocontours are also shown in the  $f_{2L}, f_{2R}$  projection.

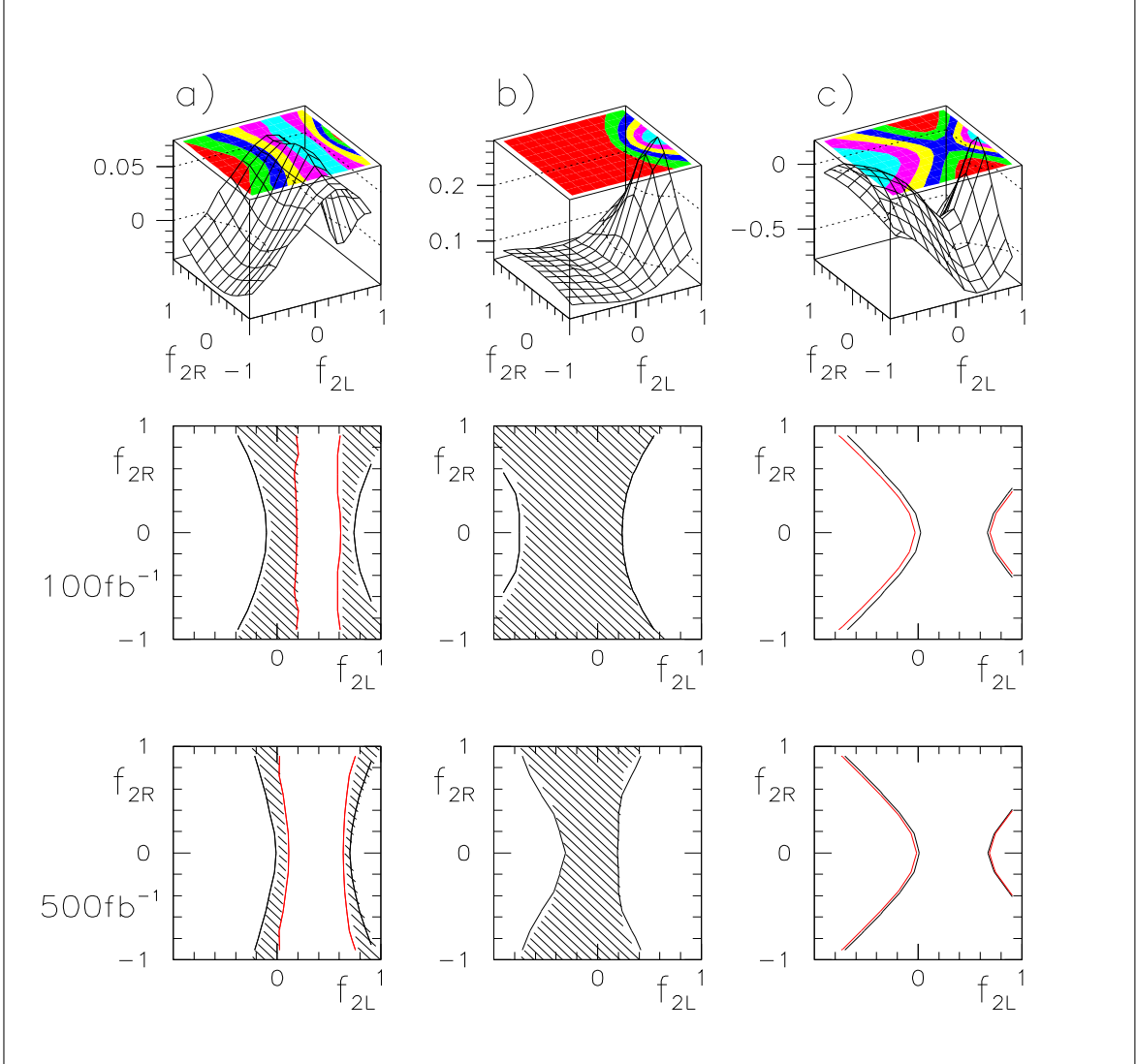


Figure 3: a) Forward-backward  $b$ -quark asymmetry in the top rest frame, b) forward-backward lepton asymmetry in the  $e^+e^-$  c.m.s. and c) energy asymmetry for the lepton in the top rest frame, as functions of  $f_{2L}$  and  $f_{2R}$ , for the reaction  $e^+e^- \rightarrow t\bar{t} \rightarrow tl^-\bar{\nu}_l\bar{b}$  at  $\sqrt{s} = 500$  GeV. Also shown are the  $2\sigma$  limits on the anomalous couplings of each observable (shaded), for integrated luminosities of  $100 \text{ fb}^{-1}$  and  $500 \text{ fb}^{-1}$ , and  $A_{FB}^b$  ( $A_{FB}^l$ ,  $A_E^l$ )-equidistant isocontours in the  $f_{2L}$ ,  $f_{2R}$  projection.

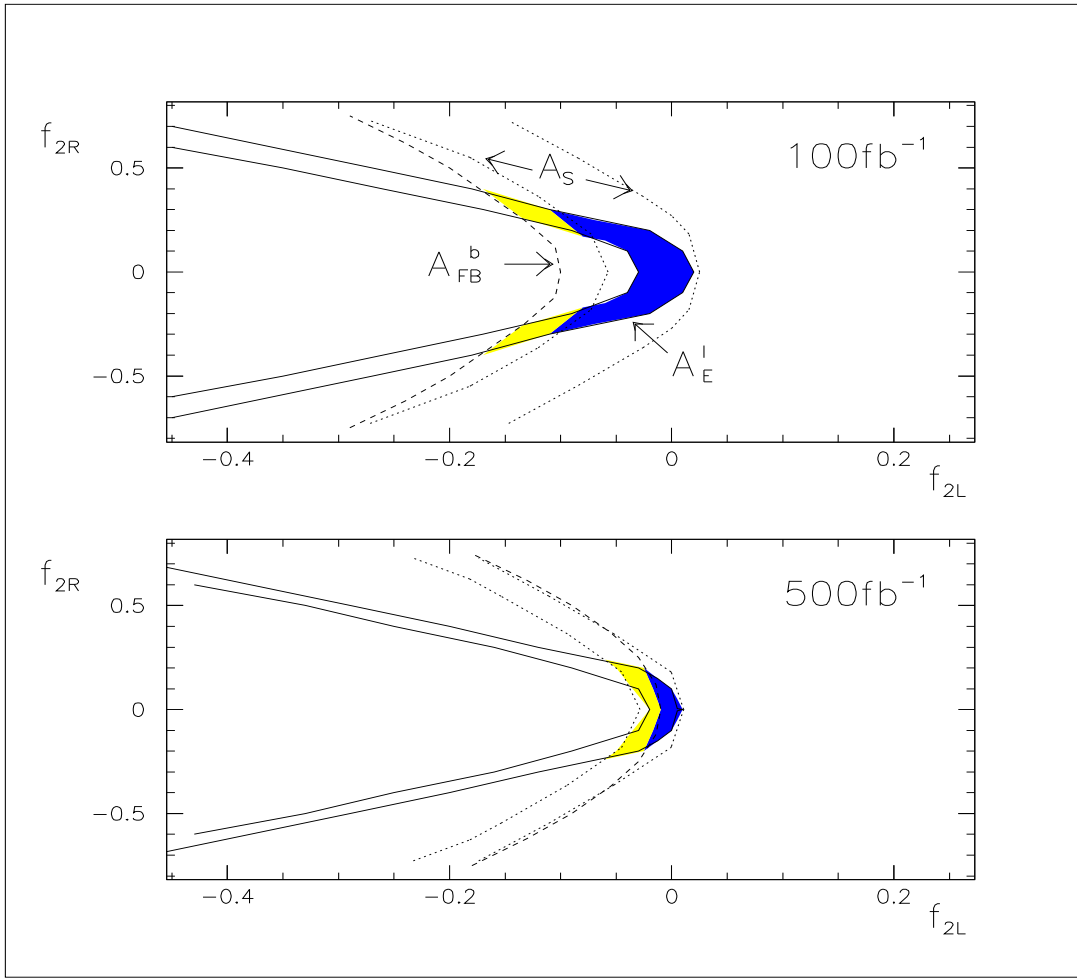


Figure 4: Combined  $2\sigma$  limits on the anomalous couplings  $f_{2L}$  and  $f_{2R}$  of the reaction  $e^+e^- \rightarrow t\bar{t} \rightarrow t l^- \bar{\nu}_l \bar{b} ((l^- \bar{\nu}_l \bar{b})(W^+b))$  at  $\sqrt{s} = 500$  GeV, for  $100 \text{ fb}^{-1}$  and  $500 \text{ fb}^{-1}$  integrated luminosities. For the meaning of the gray and dark areas we refer to the text.

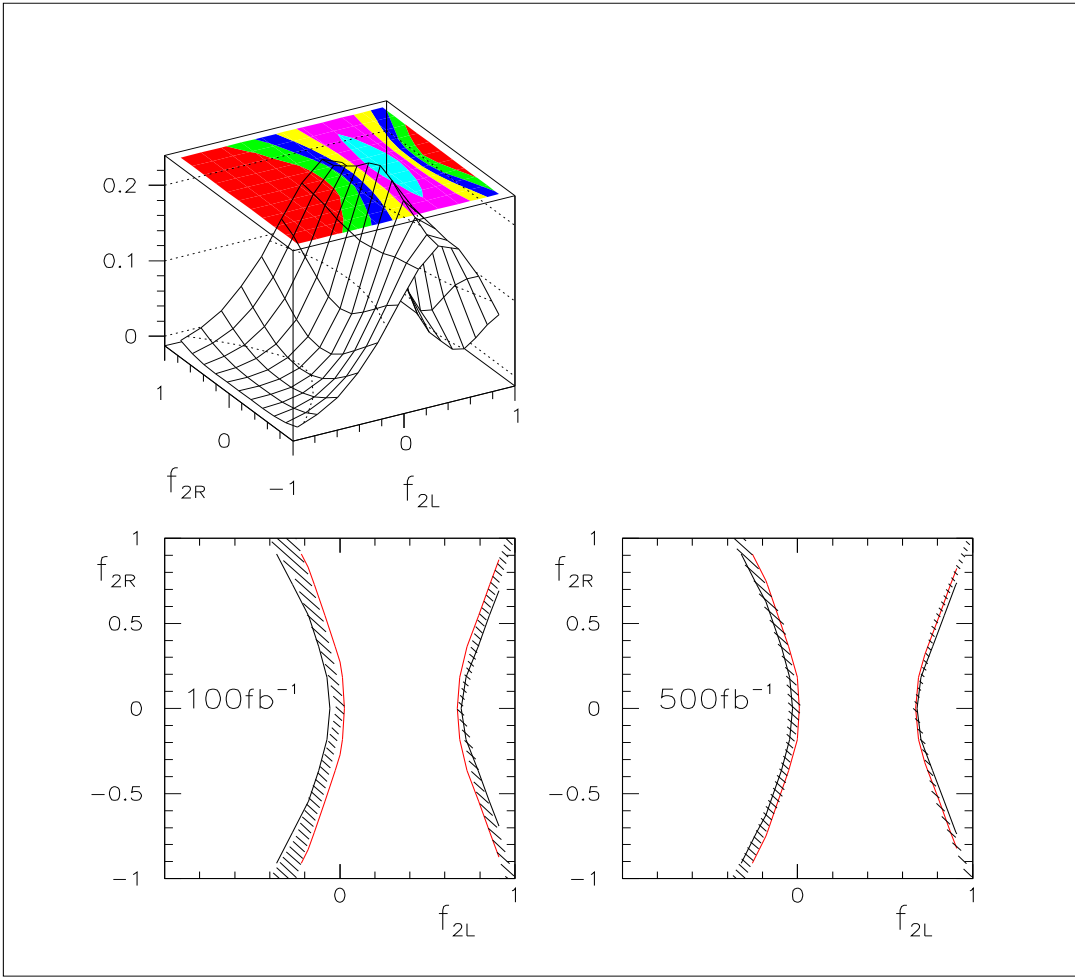


Figure 5: Spin-spin asymmetry for the  $b$ -quark in the top rest frame as a function of  $f_{2L}$  and  $f_{2R}$  for the reaction  $e^+e^- \rightarrow t\bar{t} \rightarrow (l^-\nu_l\bar{b})(u\bar{d}b)$  at  $\sqrt{s}=500$  GeV. Also shown are the  $2\sigma$  limits on the anomalous couplings (shaded) for  $100 \text{ fb}^{-1}$  and  $500 \text{ fb}^{-1}$  integrated luminosity and  $A_S^b$ -equidistant isocontours in the  $f_{2L}, f_{2R}$  projection.

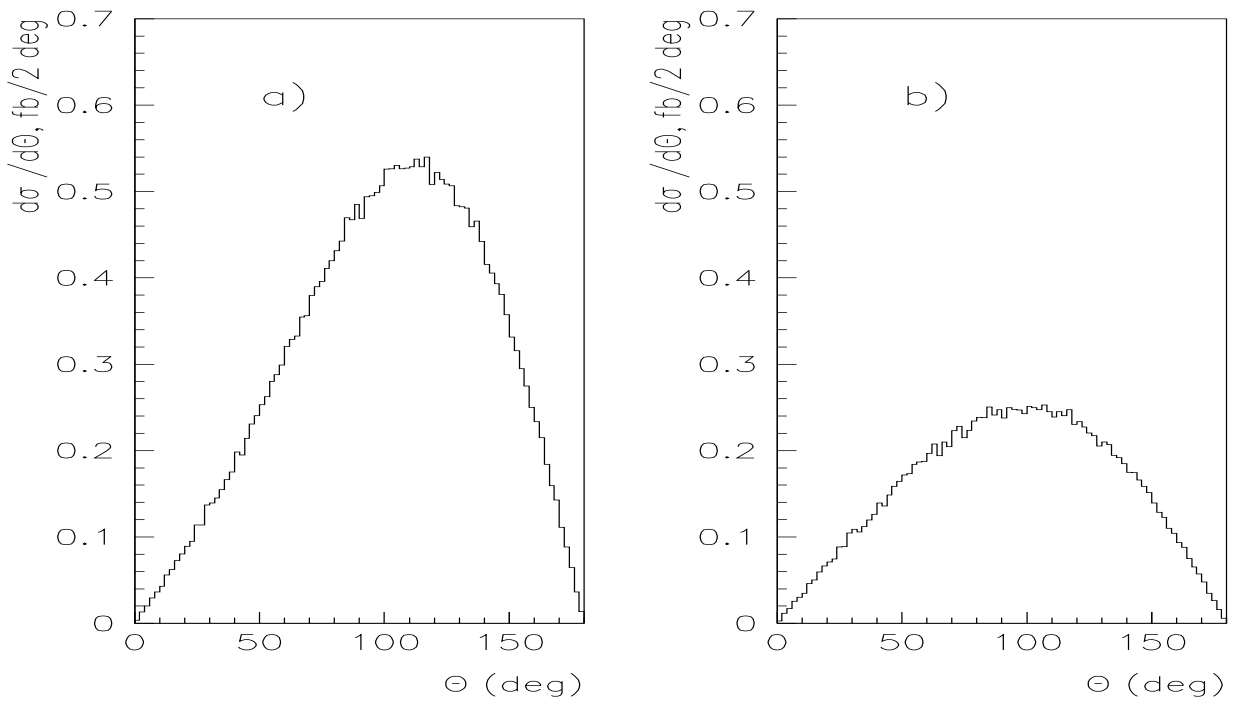


Figure 6: Angular distribution between the muon and the top in the top rest frame under the conditions that the angle between the  $\bar{d}$  and the  $\bar{t}$  in the  $\bar{t}$  rest frame is less than  $90^\circ$  and a) the top is produced in the forward hemisphere or b) the top is produced in the backward hemisphere, for the reaction  $e_L^+ e^- \rightarrow \mu^- \bar{\nu}_\mu b u \bar{d} \bar{b}$  with longitudinally polarized electrons at  $\sqrt{s} = 500$  GeV.